Optomechanically induced transparency and absorption in hybridized optomechanical systems

B. P. Hou,[1] L. F. Wei,[2] and S. J. Wang[3]

[1]*College of Physics and Electronic Engineering, Institute of Solid Physics, Sichuan Normal University, Chengdu 610101, People's Republic of China*

[2]*Laboratory of Quantum Opt-electronic Information, Southwest Jiaotong University, Chengdu 610031, People's Republic of China*

[3]*Department of Physics, Sichuan University, Chengdu 610064, People's Republic of China*

(Received 24 July 2014; revised manuscript received 2 February 2015; published 16 September 2015)

We present the normal-mode splitting and optomechanically induced transparency or absorption phenomena in the strongly tunnel-coupled optomechanical cavities. In the probe output spectrum, there appear central transparency windows or absorption peaks around which two broad sidebands are symmetrically located. It has been confirmed by the quantitative findings that two broad sidebands, which include the distorted absorption peaks, indicate the normal-mode splitting of the two hybridized cavities, and central transparency windows or absorption peaks character the interference induced by the optomechanical interactions. Additionally, the switching from absorption to amplification can be realized by only adjusting the tunnel interaction. These spectrum properties can be used for the coherent control of light pulses via microfabricated optomechanical arrays.

DOI: 10.1103/PhysRevA.92.033829 PACS number(s): 42.50.Pq, 42.50.Gy, 42.50.Wk, 42.50.Ct

I. INTRODUCTION

A cavity optomechanical system (OMS) is usually constituted by a fixed mirror and another movable mirror which is coupled to the optical field in the cavity by the radiation pressure [1,2]. It is well known that the OMS possesses many potential applications, e.g., to get the stationary entanglement between two macroscopic oscillators and two cavity fields [3–6], to cool the mechanical vibrations to their quantum ground states [7–9], to demonstrate quantum nonlinearities [10–13], to manipulate optomechanical chaos via a bichromatic driving [14], and to demonstrate the optomechanically induced transparency (OMIT) [15–17] and optomechanically induced absorption (OMIA) [18] phenomena.

The primary OMS has been generalized to the two-optical-mode system, which has attracted a lot of interest due to rich physics. For example, a scheme to produce Einstein-Podolsky-Rosen (EPR) entangled beams in an OMS consisting of a whispering-gallery mode cavity with a movable boundary was proposed [19]. The intensity correlations of the two optical fields have been studied in the OMS consisting of two tunnel-coupled optical cavity modes in which a mechanical oscillator is coupled to one of the cavity modes by radiation pressure [20]. In a two-optical-mode OMS with two cavities sharing a common membrane or oscillator, cooling to quantum mechanical ground state, enhanced quantum nonlinearities, quantum limit for probing mechanical energy quantization, and optical bistability have also been explored [9,12,21,22]. Another generalized scheme of the OMS is that two oscillating mirrors or two membranes are coupled to a common optical cavity mode. Here, the OMS with two dielectric membranes suspended in a Fabry-Perot cavity was used to generate steady-state entanglement of the mechanical vibrations between the two dielectric membranes [4,23]. Typically, in the more complicated optomechanical scheme composed by two optical modes and two mechanical ones, the entanglement of two movable mirrors [3,4,6], the phonon-photon translator [24], and the strong interaction between single photon and phonon for the quantum information processing applications [25], have been investigated.

As we well know, an absorbing atomic medium driven by a strong coupling field may be transparent for a weak probe laser. This is the phenomenon of electromagnetically induced transparency (EIT) in coherent multilevel systems [26]. Recently, the optomechanically induced transparency phenomenon (OMIT) has also been demonstrated in a simple OMS theoretically [15] and experimentally [16,17], respectively. In such an OMS, OMIT with higher-order sidebands [27] and in the nonlinear quantum regime [28–30] were studied. Furthermore, OMIT in a quadratically nanomechanical system, realized by placing a membrane in the cavity, has also been demonstrated theoretically [31] and experimentally [32], respectively. In addition, optomechanically induced absorption (OMIA) was predicted in a hybrid optoelectromechanical system [18]. In addition, the optomechanical analog of double OMIT in a hybrid optomechanical system consisting of a cavity and a mechanical resonator with a two-level system was studied [33].

Comparing with single-mode OMS, the two-mode system can provide much more flexible controllability, such as in quantum memory [34] and in coherent optical wavelength conversion [35]. In such OMS, OMIT, and OMIT-like cooling were theoretically demonstrated [36,37]. The double OMIT in the optomechanical cavity coupled to a charged nanomechanical resonator via Coulomb interaction was investigated [38]. Recently, OMIT as well as its influences by mechanical mode and the nonlinear crystal in an optomechanical cavity with two moving mirrors has been discussed [39].

On the other hand, the strong coupling between quantum systems receives much concern. The strong coupling between quantum systems is required to make their quantum dynamics dominate over the decoherence in the demonstration of the quantum properties, such as entanglement and quantum information processing. A familiar characteristic of strongly coupled systems is the occurrence of normal-mode splitting (NMS), thus the observation of the NMS provides unambiguous evidence for the strong coupling between quantum systems. For example, the NMS in cavity optomechanics due to the coupling between the fluctuations of the cavity field and the

mechanical oscillator mode was analyzed [40]. Subsequently, the optomechanical NMS for identifying the strong coupling of a cavity to a mechanical resonator was observed [41]. And, the features of NMS and OMIT in corresponding mechanical-mode splitting regime in the two-mode optomechanical system were identified [42].

In this paper, the phenomena of the OMIT or OMIA as well as the NMS phenomenon in the strongly tunnel-coupled optomechanical cavities will be investigated. The model under our consideration possesses many potential applications, e.g., to use the strong interaction between single photon and phonon in the quantum information processing [25], and to get quantum entanglement between two macroscopic mechanical resonators [6]. Here, we not only present the OMIT or OMIA interference phenomena induced by the optomechanical interactions, but also display the NMS reflecting the strong coupling between the two cavities in this system. Additionally, the spectrum properties can well distinguish these three interactions: the optomechanical interactions in the probed cavity and in the tunnel-coupled cavity, and the tunnel interaction between the cavities. This can be used for coherent control of light pulses via microfabricated optomechanical arrays.

The paper is organized as follows: In Sec. II we describe the model and solve its dynamical equation. The NMS in two coupled bare cavities is displayed in Sec. III. The OMIT and OMIA induced by a single optomechanical interaction, which is accompanied by NMS induced by the strong tunnel coupling, in two coupled cavities is discussed in Sec. IV. OMIT with a three-window structure in two strongly tunnel-coupled optomechanical cavities is given in Sec. V. Finally, in Sec. VI we summarize our main results.

II. MODEL AND ITS DYNAMICAL EQUATION

The optomechanical system considered here is shown in Fig. 1. It consists of two OMSs, each of which is constructed by two fixed end mirrors and a movable one located at the node of the cavity. The two cavities are coupled with the tunneling strength J, which is proportional to the transmittance of the two fixed mirrors of the cavities. The left and right fixed end mirrors of the cavities are, respectively, driven by two control fields. The amplitudes of the driving fields read $E_{L1} = \sqrt{2P_{L1}\kappa_1/\hbar\omega_{L1}}$ and $E_{L2} = \sqrt{2P_{L2}\kappa_2/\hbar\omega_{L2}}$, respectively. ω_{Li} $(i = 1,2)$ is the frequency of the ith control field and L_i the length of the ith cavity. Here κ_i is the field decay of the ith cavity. Meanwhile, a probe field, with the amplitude $E_p = \sqrt{2P_p\kappa_1/\hbar\omega_p}$ and the frequency ω_p, is applied on the left fixed end mirror to detect the transparency properties of the OMS. The powers of the probe and coupling fields are denoted by P_p and P_{Li} $(i = 1,2)$, respectively.

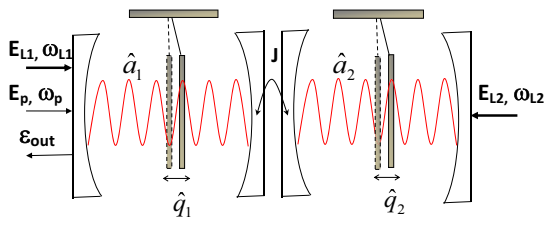

FIG. 1. (Color online) Schematic diagram of two coupled optomechanical cavities. A movable mirror is located at the middle position of each cavity which is driven by a strong control field. Additionally, the left cavity is probed by a weak field.

The Hamiltonian of the above coupled OMSs in the rotating frame at the frequency ω_{Li} of the control fields reads [6,25]

$$\begin{aligned} H = & \sum_{i=1,2} \hbar\Delta_{ci}\hat{a}_i^\dagger\hat{a}_i + \sum_{i=1,2}\left(\frac{\hat{p}_i^2}{2m_i} + \frac{1}{2}m_i\omega_{mi}^2\hat{q}_i^2\right) \\ & - \sum_{j=1,2}\hbar g_j\hat{a}_j^\dagger\hat{a}_j\hat{q}_j - \hbar J(\hat{a}_1^\dagger\hat{a}_2 e^{i\Delta_L t} + \hat{a}_2^\dagger\hat{a}_1 e^{-i\Delta_L t}) \\ & + i\hbar E_p(\hat{a}_1^\dagger e^{-i\delta t} - \hat{a}_1 e^{i\delta t}) - \sum_{i=1,2} i\hbar E_{Li}(\hat{a}_i^\dagger - \hat{a}_i), \end{aligned} \tag{1}$$

with $\delta = \omega_p - \omega_{L1}$ and $\Delta_L = \omega_{L1} - \omega_{L2}$. Here, $\Delta_{ci} = \omega_{ci} - \omega_{Li}$ $(i = 1,2)$ is detuning of the control field from the corresponding cavity, and $g_i = \frac{\omega_{ci}}{L_i}(i = 1,2)$ the optomechanical coupling between the cavity field (with ω_{ci} being the resonant frequency of the ith cavity) and the movable mirror. $\hat{a}_i$ $(\hat{a}_i^+)$ is the annihilation (creation) operator of the ith cavity field, and the operators $\hat{q}_i$ and $\hat{p}_i$ represent the position and momentum of the ith movable mirror (with the mass m_i and frequency ω_{mi}), respectively. The Heisenberg equations for the mirror and the cavity variables, including the corresponding noise and damping terms, can be written as follows:

$$\dot{\hat{q}}_i = \frac{\hat{p}_i}{m_i},\ i = 1,2, \tag{2a}$$

$$\dot{\hat{p}}_i = -m_i\omega_{mi}^2\hat{q}_i + \hbar g_i\hat{a}_i^\dagger\hat{a}_i - \gamma_{mi}\hat{p}_i + \hat{\xi}_i,\ i = 1,2, \tag{2b}$$

$$\begin{aligned} \dot{\hat{a}}_1 = & -i\Delta_{c1}\hat{a}_1 + ig_1\hat{a}_1\hat{q}_1 + iJe^{i\Delta_L t}\hat{a}_2 + E_p e^{-i\delta t} \\ & + E_{L1} - \kappa_1\hat{a}_1 + \sqrt{2\kappa_1}\hat{a}_{in,1}, \end{aligned} \tag{2c}$$

$$\begin{aligned} \dot{\hat{a}}_2 = & -i\Delta_{c2}\hat{a}_2 + ig_2\hat{a}_2\hat{q}_2 + iJe^{-i\Delta_L t}\hat{a}_1 + E_{L2} - \kappa_2\hat{a}_2 \\ & + \sqrt{2\kappa_2}\hat{a}_{in,2}. \end{aligned} \tag{2d}$$

Here, γ_{mi} and $\hat{\xi}_i$ are the damping rate and the Langevin force arising from the interaction of the ith movable mirror with environment, and $\hat{a}_{in,i}$ $(i = 1,2)$ the input vacuum in the ith cavity with zero mean value. Here the control field is much stronger than the probe field; we could use the linearization approach of quantum optics to get an analytical understanding. After dividing the variables into the steady parts and the fluctuation ones, $\hat{q}_i = q_{is} + \delta\hat{q}_i, \hat{p}_i = p_{is} + \delta\hat{p}_i, \hat{a}_i = a_{is} + \delta\hat{a}_i$ $(i = 1,2)$, the dynamical behaviors of the system can be obtained by solving the equation of motion for the fluctuations $(\delta\hat{q}_i, \delta\hat{p}_i, \delta\hat{a}_i)$ around their steady-state parts (q_{is}, p_{is}, a_{is}).

Substituting the division forms into Eqs. (2a)– (2d) and assuming the control fields are stronger than the probe field, the steady solutions of the above dynamical equations can be obtained as

$$p_{is} = 0, \quad i = 1,2, \tag{3}$$

$$q_{is} = \frac{\hbar g_i|a_{is}|^2}{m_i\omega_{mi}^2}, \quad i = 1,2, \tag{4}$$

$$a_{\alpha s} = \frac{E_{L\alpha}(\kappa_\beta + i\Delta_\beta) + iJE_{L\beta}e^{i(-1)^{\alpha+1}\Delta_L t}}{J^2 + (\kappa_\alpha + i\Delta_\alpha)(\kappa_\beta + i\Delta_\beta)}, \quad (\alpha,\beta = 1,2,\alpha \neq \beta), \tag{5}$$

where $\Delta_\alpha = \Delta_{c\alpha} - g_\alpha q_{\alpha s}$ $(\alpha = 1,2)$ is the effective detuning and $|a_{is}|^2$ the ith cavity intensity. Without loss of the generality, we assume that the frequency of the left control field is identical to the right one, i.e., $\Delta_L = 0$. As all the control fields are assumed to be sufficiently strong, all the operators can be identified with their expectation values. Then, the Langevin equations for the expectation values $(\delta q_i, \delta p_i, \delta a_i)$ of the fluctuations $(\delta\hat{q}_i, \delta\hat{p}_i, \delta\hat{a}_i)$ can be linearized as

$$\delta\dot{q}_i = \frac{\delta p_i}{m_i}, \quad i = 1,2, \tag{6a}$$

$$\delta\dot{p}_i = -m_i\omega_{mi}^2\delta q_i + \hbar g_i a_{is}^*\delta a_i + \hbar g_i a_{is}\delta a_i^* - \gamma_{mi}\delta p_i, \quad i = 1,2, \tag{6b}$$

$$\delta\dot{a}_1 = -i\Delta_{c1}\delta a_1 + ig_1 a_{1s}\delta q_1 + ig_1 q_{1s}\delta a_1 + iJe^{i\Delta_L t}\delta a_2 + E_p e^{-i\delta t} - \kappa_1\delta a_1, \tag{6c}$$

$$\delta\dot{a}_2 = -i\Delta_{c2}\delta a_2 + ig_2 a_{2s}\delta q_2 + ig_2 q_{2s}\delta a_2 + iJe^{-i\Delta_L t}\delta a_1 - \kappa_2\delta a_2. \tag{6d}$$

To discuss EITs in the present coupled optomechanical systems, we need only investigate the response of the probe field. Using the following ansatz (in the rotating frame),

$$\begin{aligned}\delta q_i &= q_{i+}e^{-i\delta t} + q_{i-}e^{i\delta t},\\ \delta p_i &= p_{i+}e^{-i\delta t} + p_{i-}e^{i\delta t},\\ \delta a_i &= a_{i+}e^{-i\delta t} + a_{i-}e^{i\delta t}.\end{aligned} \tag{7}$$

In the resolved sideband regime of $\omega_{mi} > \kappa_i$, $(i = 1,2)$ and under the condition of $\Delta_i = \omega_{mi}$ $(i = 1,2)$ [15–17], the component of the output field, oscillating at the probe frequency ω_p, is given by

$$\varepsilon_{out} = \frac{2\kappa_1 a_{1+}}{E_p} = \frac{2\kappa_1\Lambda G_{2+}}{G_{2+}(Q_{1+}\Lambda - Q_{2-}^* B_1) + iJG_{1+}(A_1 - \Lambda)}, \tag{8}$$

$$= \frac{2\kappa_1}{Q_{1+} - \frac{B_1}{Q_{1-}^* + \frac{J^2}{Q_{2-}^*}} + \frac{J^2}{\Lambda}\frac{(\Lambda - A_1)(\Lambda - A_2)}{Q_{2+}\Lambda - B_2^* Q_{1-}^*}}. \tag{9}$$

Here,

$$\begin{aligned} G_{1+} &= \frac{iJQ_{2-}^*}{\Lambda}(\Lambda - A_2),\\ G_{2+} &= Q_{2+}Q_{2-}^* + \frac{B_2}{\Lambda}(J^2 - \Lambda),\\ \Lambda &= Q_{1-}^* Q_{2-}^* + J^2,\\ A_1 &= g_1 g_2 a_{1s} a_{2s}^* M_{1-}^* M_{2+},\\ A_2 &= g_1 g_2 a_{1s}^* a_{2s} M_{1+} M_{2-}^*,\\ B_j &= g_j^2 |a_{js}|^2 M_{j+} M_{j-}^*,\\ Q_{j\alpha} &= \mu_{j\alpha} - ig_j a_{js} M_{j\alpha}, (\alpha = +,-), \end{aligned} \tag{10}$$

and

$$\begin{aligned} M_{j+} &= \frac{\hbar g_j a_{js}^*}{m_j\Omega_j},\\ M_{j-} &= \frac{\hbar g_j a_{js}^*}{m_j\Omega_j^*},\\ \mu_{j+} &= \gamma_j + i\Delta_j,\\ \mu_{j-} &= \gamma_j^* + i\Delta_j,\\ \Omega_j &= \omega_{mj}^2 - i\delta\Gamma_j, \end{aligned} \tag{11}$$

with $j = 1,2$, $\gamma_j = \kappa_j - i\delta$, and $\Gamma_j = \gamma_{mj} - i\delta$. Note that the terms related to J in Eq. (9) represent the tunnel contributions to the probe output laser from the right optomechanical system. Physically, the absorption property of the probe field is described by the real part ε_R of the output field ε_{out} at the probe frequency.

III. NORMAL-MODE SPLITTING IN TWO COUPLED BARE CAVITIES

First we investigate the normal-mode splitting (NMS) in the probe spectrum for two coupled bare cavities. To make the following result within experimental realizations, we use the parameters in a recent experiment for the observation of the NMS [15,41]: the wavelength of the control field $\lambda_1 = \lambda_2 = 2\pi c/\omega_L = 1064$ nm with $\omega_{L1} = \omega_{L2} = \omega_L$, $L_1 = L_2 = 25$ mm, $\kappa_1 = \kappa_2 = 2\pi \times 215$ kHz, $\omega_{m1} = \omega_{m2} = 2\pi \times 947$ kHz, $m_1 = m_2 = 145$ ng, $\omega_{c1} = \omega_{c2} = 1.77 \times 10^{15}$ Hz, and $\gamma_{m1} = \gamma_{m2} = 2\pi \times 140$ Hz.

If two degenerate bare cavities with resonance frequency ω_c $(\omega_{c1} = \omega_{c2} = \omega_c)$ and decaying rate κ $(\kappa_1 = \kappa_2 = \kappa)$ are weakly coupled for $J < \kappa$, there appears only a single resonance around $\sigma = 0$ in the probe output spectrum (not shown by figures). When the tunnel coupling between the two cavities is increased up into the strong regime, i.e., $J \geqslant \kappa$, the two degenerate cavity modes are hybridized and split into two normal modes with resonant frequencies $\omega_c \pm J$, which are separated by $2J$. For example, when the tunnel coupling is set as $J = \kappa$, 3κ, and 5κ shown by solid, dashed, and dotted curves in Fig. 2, there appears a splitting in the probe spectrum and its separation increases linearly with the tunnel coupling J. This can be explained by calculating the degeneracy frequencies of the normal modes. Instead, we here use the probe output spectrum, which includes the decays of the cavities, to demonstrate the NMS displayed by Fig. 2. When the two control fields are switched off $(E_{L1} = E_{L2} = 0)$, Eq. (8) or (9) can be simplified as

$$\varepsilon_{\text{out}} = \frac{2\kappa_1}{\kappa_1 - i(\delta - \omega_{m1}) + J^2/[\kappa_2 - i(\delta - \omega_{m2})]}. \tag{12}$$

Then the real part ε_R of the probe output field, representing the absorption properties of the probe field, is easily obtained as

$$\varepsilon_R = \frac{2\kappa^2(\kappa^2 + \sigma^2 + J^2)}{\sigma^4 + 2\sigma^2(\kappa^2 - J^2) + (\kappa^2 + J^2)^2}, \tag{13}$$

with $\sigma = \delta - \omega_m$ and $\kappa_1 = \kappa_2 = \kappa$. Two resonance peaks corresponding to the two normal modes are located at

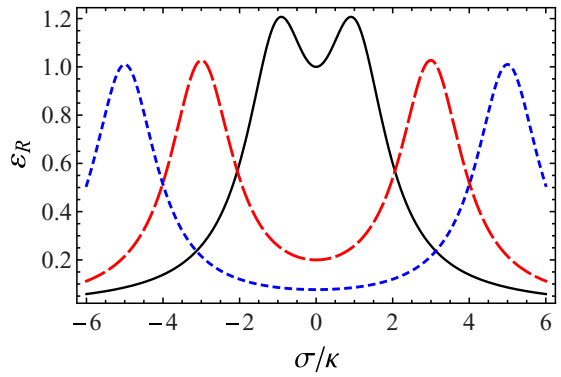

FIG. 2. (Color online) Real part (absorption) of the output field ε_{out} as a function of the normalized frequency σ/κ in the case of $E_{L1} = E_{L2} = 0$ ($P_{L1} = P_{L2} = 0$) for different tunnel coupling: $J = \kappa$ (black, solid curve); $J = 3\kappa$ (red, dashed curve); $J = 5\kappa$ (blue, dotted curve). The values of the parameters are given by $L_1 = L_2 = L = 25$ mm, $\omega_{c1} = \omega_{c2} = 1.77 \times 10^{15}$ Hz, $\kappa_1 = \kappa_2 = \kappa = 2\pi \times 215$ kHz.

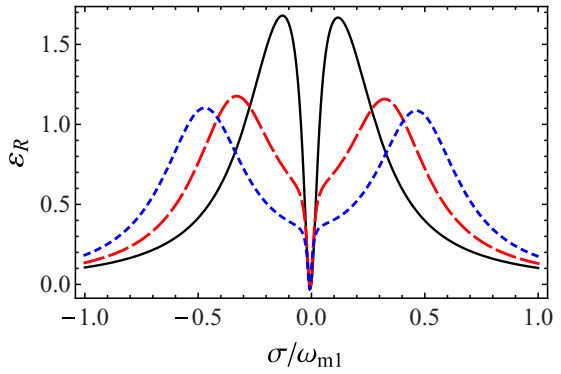

FIG. 3. (Color online) Real part (absorption) of the output field ε_{out} as a function of the normalized frequency σ/ω_{m1} when only considering the optomechanical interaction in the probed cavity, which is coupled to a bare cavity. The tunnel coupling is set as different values: $J = 0.5\kappa$ (black, solid curve); $J = 1.4\kappa$ (red, dashed curve); $J = 2\kappa$ (blue, dotted curve). The values of the parameters are given by $P_{L1} = 3$ mW, $P_{L2} = 0$ mW, $\lambda_1 = \frac{2\pi c}{\omega_{L1}} = 1064$ nm, $\omega_{m1} = 2\pi \times 947$ kHz, and $\gamma_{m1} = 2\pi \times 140$ Hz. Other parameters are the same as those in Fig. 2.

$\sigma_\pm = \pm\sqrt{-(J^2+\kappa^2) + 2J\sqrt{J^2+\kappa^2}} \approx \pm J$ and their separation is given by $\sigma_+ - \sigma_- \approx 2J$. Specifically, we have $\sigma_\pm \approx \pm 2.996\kappa$ for $J = 3\kappa$. This is coincident with the results shown by the dashed curve in Fig. 2.

IV. OPTOMECHANICALLY INDUCED TRANSPARENCY AND ABSORPTION INDUCED BY A SINGLE OPTOMECHANICAL INTERACTION IN TWO COUPLED CAVITIES

In the following, we shall discuss the interference phenomena induced by an optomechancial cavity which is coupled to another bare cavity. First, we can recur the usual OMIT in a single-mode OMS only by switching off the tunnel coupling between the two cavities. At this time, the right optomechanical cavity is decoupled from the left one; the present OMIT spectrum is independent of the parameters related to the right cavity. And the probe output spectrum in Eq. (9) is reduced to the form of the single optomechanical system, i.e., $\varepsilon_{\text{out}} = 2\kappa_1/(Q_{1+} - B_1/Q_{1-}^*)$.

Now we consider the output spectrum induced by the optomechanical interaction in the probed cavity which is coupled to a bare cavity. In Fig. 3, we plot solid, dashed, and dotted curves for $J = 0.5\kappa$, 1.4κ, and 2κ, respectively. It is shown from solid curve that the probe spectrum displays the OMIT feature similar to that in a single-mode OMS. In this case where the two cavities are weakly coupled for $J = 0.5\kappa$, the normal modes are not split and the output spectrum is dominated by the OMIT induced by the optomechanical interaction in the probed cavity. When the tunnel coupling is tuned into a strong coupling regime, i.e., $J > \kappa$, the coupling between the two cavities can't be ignored and will influence the probe spectrum. It can be seen by dashed ($J = 1.4\kappa$) and dotted ($J = 2\kappa$) curves in Fig. 3 that the OMIT spectra become distorted; the two peaks in these two cases are bent to outer sides. This distortion indicates the evidence of the NMS induced by the strong coupling between the two cavities. This can be demonstrated by the distance between the two distorted peaks, which is contributed by the NMS induced by the strong tunnel coupling and the OMIT window resulted from the optomechanical interaction in the probe cavity. Specifically, the separation between the distorted peaks is given by $2(J + \Gamma_{\text{OM1}})$, in which the width of the central transparency window denoted by Γ_{OM1} in the probe spectrum is given by

$$\Gamma_{\text{OM1}} \approx \frac{\gamma_{m1}}{2} + \frac{G_{\text{OM1}}}{\kappa_1}. \tag{14}$$

The optomechanical coupling in the probe cavity is given by $G_{\text{OM1}} = x_{10}^2 g_1^2 |a_{1s}|^2$ with $x_{10} = \sqrt{\hbar/2m_1\omega_1}$ being the spread of the ground-state wave function of the mechanical oscillator. For example, when the values of the tunnel coupling are given by $J = 1.4\kappa$ and 2κ, we get the distances between the two distorted absorption peaks in these two cases, respectively, given by $0.64\omega_{m1}$ and $0.91\omega_{m1}$, which are well coincident with dashed and dotted curves in Fig. 3.

Next, we consider the effects of the optomechanical interaction in the tunnel-coupled cavity on the probe spectrum by switching off the left control field, instead by turning on the right control field applied on the tunnel-coupled cavity. To compare with the spectrum properties from the right control field, we present the probe spectrum in the two-coupled bare cavities, which is shown by solid curve in Fig. 4. We can see that there appears a noise resonance with a Lorentzian peak, which is broader than that of width κ ($\kappa_1 = \kappa_2 = \kappa$) for a single bare cavity. When turning on the right control field, the optomechanical interaction in the tunnel-coupled cavity emerges due to the radiation pressure induced by the control field. To display the effects of the optomechanical interaction in the tunnel-coupled cavity on the probe spectrum, we tune the tunnel coupling between the two cavities into a weak coupling regime, i.e., $J < \kappa$. From the dashed curve for $J = 0.5\kappa$ in Fig. 4, it is exhibited that there appears a absorption peak loaded on the top of the resonance spectrum shown in the solid curve. This implies that the optomechanical interaction

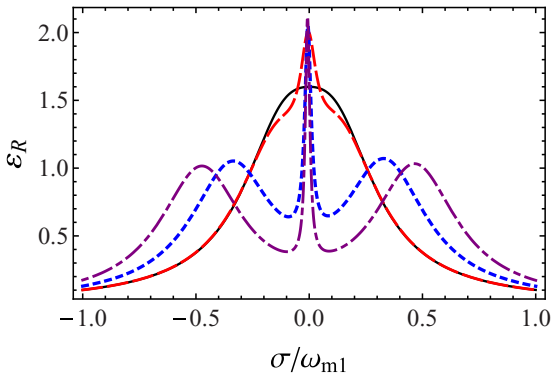

FIG. 4. (Color online) Real part (absorption) of the output field ε_{out} as a function of the normalized frequency σ/ω_{m1} when only considering the optomechanical interaction in the tunnel-coupled cavity. The right control field and the tunnel coupling are set as different values: $J = 0.5\kappa$, $P_{L2} = 0$ (black, solid curve); $J = 0.5\kappa$, $P_{L2} = 3$ mW (red, dashed curve); $J = 1.4\kappa$, $P_{L2} = 3$ mW (blue, dotted curve); $J = 2\kappa$, $P_{L2} = 3$ mW (purple, dashed-dotted curve). The values of the parameters are given by $P_{L1} = 0$ mW, $\lambda_2 = \frac{2\pi c}{\omega_{L2}} =$ 1064 nm, $\omega_{m2} = 2\pi \times 947$ kHz, and $\gamma_{m2} = 2\pi \times 140$ Hz. Other parameters are the same as those in Fig. 2.

in the tunnel-coupled cavity leads to the appearance of the optomechanically induced absorption (OMIA) in the probe spectrum.

It is natural to wonder how this probe absorption spectrum behaves when the tunnel coupling between the two cavities is tuned into the strong regime, i.e., $J > \kappa$. From dotted ($J = 1.4\kappa$) and dotted-dashed ($J = 2\kappa$) curves in Fig. 4, we can see that besides a sharp absorption peak is located at $\sigma = 0$, two symmetrical sideband windows are produced by the strong tunnel coupling. When increasing the tunnel coupling, the sideband windows become deeper and wider. The occurrence of the sideband windows indicates the evidence of the NMS in the hybridized cavity modes. This can be confirmed by investigating the distance between the sideband peaks, which consists of the widths of the sideband windows and the bandwidth of the central absorption peak. The widths of the sideband windows depend linearly on the coupling rate J, and the bandwidth of the central absorption peak is given by Γ_{OM2}. In the strong tunnel coupling regime ($J > \kappa_1, \kappa_2$) and under the assumption of $\gamma_{m2} \ll \kappa_2$, the bandwidth of the central absorption peak is given by

$$\Gamma_{OM2} \approx \frac{\kappa_1 G_{OM2}}{\sqrt{J^4 - \kappa_1^2 \kappa_2^2}}, \tag{15}$$

in which $G_{OM2} = x_{20}^2 g_2^2 |a_{2s}|^2$ denotes the optomechanical coupling in the tunnel-coupled cavity, and $x_{20} = \sqrt{\hbar/2m_2\omega_2}$ is the spread of the ground-state wave function of the mechanical oscillator. For $J = 1.4\kappa$ and 2κ, we can get the distances between the sideband peaks as $2(J + \Gamma_{OM2}) \approx 0.69\omega_1$ and $0.94\omega_1$, which are coincident well with the dotted and dashed-dotted curves in Fig. 4, respectively. This further indicates that the sideband windows reveal the appearance of the NMS induced by the strong tunnel coupling. Therefore, the spectrum features displayed by dotted and dotted-dashed curves in Fig. 4 are just the juxtaposition of the OMIA induced by the optomechanical interaction in the tunnel-coupled cavity and the NMS caused by the strong tunnel coupling.

V. OPTOMECHANICALLY INDUCED TRANSPARENCY IN TWO STRONGLY COUPLED OPTOMECHANICAL CAVITIES

The distinct difference between the features shown by Figs. 3 and 4 in Sec. IV is that an OMIT dip at $\sigma = 0$ is created by the optomechanical interaction in the probed cavity, while an OMIA peak is produced by the optomechanical interaction in the tunnel-coupled cavity. It is interesting to wonder about the effects of the two optomechanical interactions in both the cavities on the probe spectrum. Then we shall focus on the probe spectrum properties in the case where both the optomechanical cavities are simultaneously driven by the control fields.

First, we investigate the variation of the probe spectrum with the tunneling amplitude J in the presence of two optomechanical interactions. Without loss of generality, we assume that the two cavities hold the same decay rate and are driven by the control fields with identical amplitudes and wavelengths. To manifest the features in the weak or strong tunnel coupling regimes, we recur the usual OMIT in a single-mode optomechanical cavity by setting $J = 0$, which is shown by the solid curve in Fig. 5. When the tunnel coupling is tuned into a weak regime, e.g., the case for $J = 0.5\kappa$ is shown in the dashed curve, the peaks of the OMIT window become shorter and the transparency window turns shallower than the solid curve.

Now, we consider the case where the tunnel coupling is increased into a strong regime. In Fig. 5, we plot dotted ($J = 1.4\kappa$) and dashed-dotted ($J = 2\kappa$) curves with $\kappa = \kappa_1 = \kappa_2 = 2\pi \times 215$ kHz, and find that both the peaks of the central transparency window are split into broader sideband windows located symmetrically around the central window. Although the tunnel coupling is set as different values, the widths of the center OMIT windows are changed a little. This is due to the fact that the width of the central window is

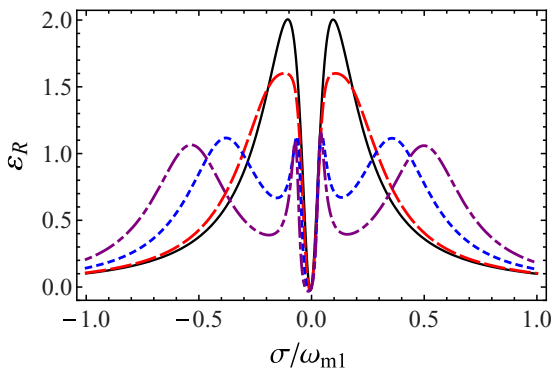

FIG. 5. (Color online) Real part ε_R (absorption) of the output field ε_{out} as a function of the normalized frequency σ/ω_{m1} with $P_{L1} = P_{L2} = 3$ mW for different tunneling amplitudes: $J = 0$ (black, solid curve); $J = 0.5\kappa$ (red, dashed curve); $J = 1.4\kappa$ (blue, dotted curve); $J = 2.0\kappa$ (purple, dashed-dotted curve). The values of the parameters are set as $\lambda_1 = \lambda_2 = \frac{2\pi c}{\omega_L} = 1064$ nm with $\omega_{L1} = \omega_{L2} = \omega_L$, $\omega_{m1} = \omega_{m2} = \omega_m = 2\pi \times 947$ kHz, and $\gamma_{m1} = \gamma_{m2} = 2\pi \times 140$ Hz. Other parameters are the same as those in Fig. 2.

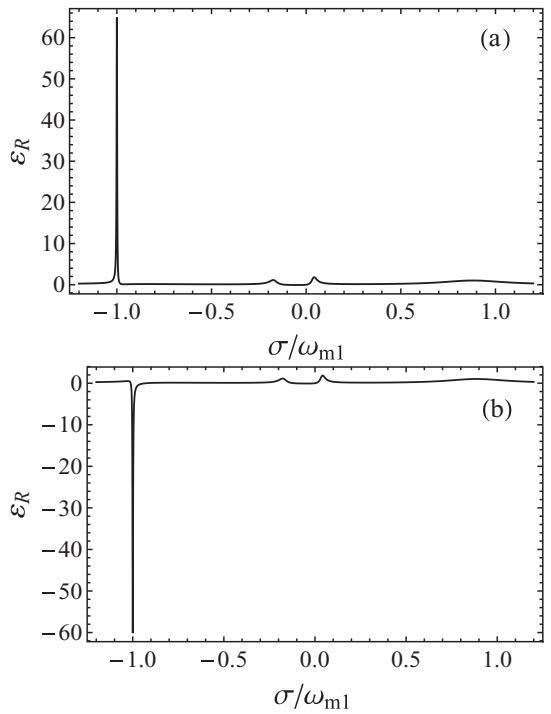

FIG. 6. Real part ε_R (absorption) of the output field ε_{out} as a function of the normalized frequency σ/ω_{m1} for different tunneling amplitudes: (a) $J = 3.50\kappa$; (b) $J = 3.52\kappa$. Other parameters are the same as those in Fig. 5.

mainly determined by the optomechanical interactions. Here, the widths of the sideband windows depend linearly on the tunnel coupling J. The appearance of the sideband windows provides an unambiguous evidence for the NMS induced by the strong tunnel coupling between the cavities. These spectrum properties will be demonstrated by the following analytical findings.

Our numerical results also show that, when $J > 3.5\kappa$ for the experimental parameters used above, the three-window OMIT spectrum is changed into an abrupt absorption or amplification line at $\sigma = -1$ (i.e., $\delta = 0$). Under this limit the probe absorption properties at $\delta = 0$ are very sensitive to the tunneling amplitude J. For example, an abrupt absorption line is obtained for $J = 3.50\kappa$ and the absorption line is turned into a deep amplification dip for $J = 3.52\kappa$ [see Figs. 6(a) and 6(b) in detail]. This suggests that a switching from absorption to amplification can be realized by just adjusting the tunneling amplitude J.

When the probe field is tuned at $\sigma = -1$ ($\delta = 0$), i.e., $\omega_p = \omega_{L1}$, the control fields drive the optomechanical cavity at the same frequency ω_L ($\omega_{L1} = \omega_{L2} = \omega_L$) as the probe field. The oscillating frequency of the intracavity field induced by the control and probe fields is far detuned from the mechanical resonance frequency, and then the resonance excitation of the mechanical oscillator is suppressed. Correspondingly, the OMIT or OMIA at $\delta = \omega_m$, which are induced by the mechanical resonance excitation, are also suppressed. On the other hand, when the optomechanical cavities are strongly driven by the control fields at ω_L, the spectrum properties for the probe field at $\sigma = -1$ ($\omega_p = \omega_{L1}$) is sensitive to the

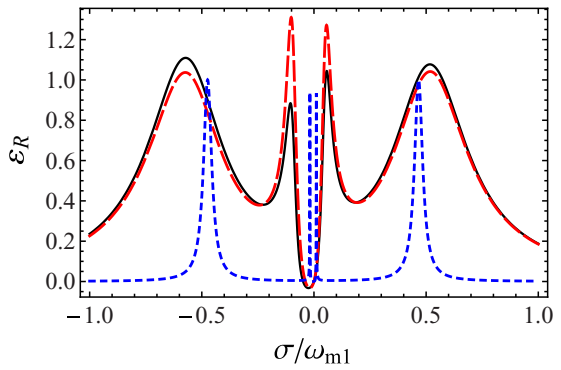

FIG. 7. (Color online) Real part ε_R (absorption) of the output field ε_{out} as a function of the normalized frequency σ/ω_{m1} with $J = 2\kappa$. The parameters are given by $P_{L1} = 6$ mW, $P_{L2} = 3$ mW, $\kappa = 2\pi \times 215$ ($\kappa_1 = \kappa_2 = \kappa$) (black, solid curve); $P_{L1} = 3$ mW, $P_{L2} = 6$ mW, $\kappa = 2\pi \times 215$ (red, dashed curve); $P_{L1} = P_{L2} = 6$ mW, $\kappa = 0.2\pi \times 215$ (blue, dotted curve). Other parameters are the same as those in Fig. 2.

intracavity field produced by the control field and the tunnel interaction. When the control field is fixed, the parametrical amplification or absorption for the probe field can be stirred by the photons fed through the tunnel coupling. For example, the probe field is strongly amplified when the tunnel coupling increases above $J_0 \approx 3.5096\kappa$, below which the probe field is absorbed.

In the following, we shall discuss the effects of the two control fields with different strengths and different cavity decay rates on the probe spectrum when the tunnel coupling is fixed. We fix the tunnel coupling at $J = 2\kappa$ and set the powers of the two control fields as $P_{L1} = 6$ mW and $P_{L2} = 3$ mW, shown by the solid curve in Fig. 7, to display the probe absorption properties in the case where the left control field is stronger than the right one. It is shown that the right peak of the central transparency window is taller than the left one. Now, we plot the dashed curve in Fig. 7 for $P_{L1} = 3$ mW and $P_{L2} = 6$ mW to show the situation in which the right control field is stronger than the left one. At this time, the left peak of the central transparency window is taller than the right one. By comparing these two curves, we can see that the peaks in the dashed curve are taller than the peaks in the solid curve. Additionally, it is found that the widths of the sideband shown in solid and dashed curves are almost unchanged, although the two control fields are set as different powers. This can be explained by investigating the expression for the distance between the sideband absorption peaks. This distance is contributed by the widths of the sideband windows and that of the central transparency window, which are given by $2(J + \Gamma_{\text{OM12}})$. Under the assumptions of $\gamma_{m1} \ll \kappa_1$ and $\gamma_{m2} \ll \kappa_2$, the width of the central transparency window is obtained as

$$\Gamma_{\text{OM12}} \approx \frac{G_{\text{OM1}} G_{\text{OM2}}}{\sqrt{J^2 + \kappa^2}} \times \frac{1}{\sqrt{\sqrt{J^2 + \kappa^2} G_{\text{OM1}}^2 + J\left(G_{\text{OM1}}^2 + G_{\text{OM1}} G_{\text{OM2}}\right)}}, \tag{16}$$

where G_{OM1} and G_{OM2} are the optomechanical couplings in the two cavities. From Eq. (16), we can obtain the distances between the sideband peaks in the cases $P_{L1} = 6$ mW, $P_{L2} = 3$ mW and $P_{L1} = 3$ mW, $P_{L2} = 6$ mW as $1.02\omega_{m1}$ and $1.00\omega_{m1}$, which are coincident well with solid and dashed curves in Fig. 7, respectively.

Now we consider the effects of the decay rates of the cavities on the probe spectrum. We decrease the decay rate of the cavity at $\kappa = 0.2\pi \times 215$ and increase the two control fields up to the same value $P_{L1} = P_{L2} = 6$ mW, which is displayed by the dotted curve in Fig. 7. It is shown that the sideband windows in this case become deeper with an identical depth to that of the central transparency window. This can be understood in terms of the discussions on the NMS in two coupled bare cavities in Sec. III, in which the width and depth for the sideband windows are mainly determined by the tunnel coupling and the cavity decay rates. Additionally, the separation between the sideband peaks becomes narrower. This is mainly due to the reduction of the central transparency window width with decrease of the cavity decay rates, which can be illustrated by using Eqs. (16) and (5). It is noted that the optomechanical couplings G_{OM1} and G_{OM2} expressed in Eq. (5) are proportional to the cavity decay rates. For example, the distance between the sideband peaks for $\kappa = 0.2\pi \times 215$ shown in the dotted curve in Fig. 7 is about $0.93\omega_{m1}$.

Finally, we predict how to achieve the tunneling coupling in excess of the cavity decay. This can be realized by reducing the cavity decay or increasing the tunnel coupling. The cavity with ultrahigh Q factors in excess of 100 million can be produced to significantly reduce the cavity decay [43,44]. On the other hand, a larger tunnel coupling can be achieved by appropriately adjusting the spacing between the cavities [45]. The coupled optomechanical cavities with the tunnel coupling in excess of the cavity decay have been used to implement the quantum information processing with photons and phonons [25].

VI. SUMMARY

We have investigated the spectrum properties of the probe output field in the two tunnel-coupled optomechanical cavities, which are, respectively, driven by the control lasers. The interference phenomena, such as OMIT and OMIA, caused by the optomechanical interactions and the NMS induced by the strong tunnel coupling between the cavities can be presented in this optomechanical system. We find that in the spectrum of a weak field probing an optomechanical cavity coupled to a bare cavity, there appears a transparency window with two absorption peaks distorted by the strong tunnel coupling between the cavities. When switching off the optomechanical interaction in the probed cavity and turning on the optomechanical interaction in the tunnel-coupled cavity, besides a sharp absorption peak at resonance is created by the optomechanical interaction, two broad sideband windows located symmetrically around the central peak are produced by the strong tunnel coupling. In the case of the simultaneous application of the two control fields, we find that there appears a spectrum with a three-window structure: A transparency window at the resonant point is created by the two optomechanical interactions, and two sideband windows located symmetrically around the central window are produced by the strong coupling between the two optomechanical cavities. The sideband windows as well as the distortion of the absorption peaks identify the NMS for the two strongly coupled cavities, and central transparency windows or absorption peaks character the optomechanical interactions. This can be used for the coherent control of light pulses via microfabricated optomechanical arrays.

ACKNOWLEDGMENTS

B.P.H. thanks J. H. An and Y. H. Zhao for valuable discussions. This work was supported partly by the National Natural Science Foundation of China (NSFC) under Grants No. 10647007, No. 10874142, and No. 10775100, and the Young Foundation of Sichuan Province, China under Grant No. 09ZQ026-008. This work is also partly supported by NSFC under Grants No. 91321104, No. 11174373, and No. U1330201, and the National Fundamental Research Program of China through Grant No. 2010CB923104.

[1] P. Meystre, Ann. Phys. (Berlin) **525**, 215 (2013).
[2] T. J. Kippenberg and K. J. Vahala, Optics Express **15**, 17172 (2007).
[3] S. Mancini, V. Giovannetti, D. Vitali, and P. Tombesi, Phys. Rev. Lett. **88**, 120401 (2002).
[4] M. J. Hartmann and M. B. Plenio, Phys. Rev. Lett. **101**, 200503 (2008).
[5] D. Vitali, S. Gigan, A. Ferreira, H. R. Bohm, P. Tombesi, A. Guerreiro, V. Vedral, A. Zeilinger, and M. Aspelmeyer, Phys. Rev. Lett. **98**, 030405 (2007).
[6] J.-Q. Liao, Q.-Q. Wu, and F. Nori, Phys. Rev. A **89**, 014302 (2014).
[7] J. Teufel, T. Donner, D. Li, J. W. Harlow, M. S. Allman, K. Cicak, A. J. Sirois, J. D. Whittaker, K. Lehnert, and R. Simmonds, Nature (London) **475**, 359 (2011).
[8] J. Chan, T. P. M. Alegre, A. H. Safavi-Naeini, J. T. Hill, A. Krause, S. Groblacher, M. Aspelmeyer, and O. Painter, Nature (London) **478**, 89 (2011).
[9] M. Bhattacharya and P. Meystre, Phys. Rev. Lett. **99**, 073601 (2007).
[10] P. Rabl, Phys. Rev. Lett. **107**, 063601 (2011).
[11] A. Nunnenkamp, K. Børkje, and S. M. Girvin, Phys. Rev. Lett. **107**, 063602 (2011).
[12] M. Ludwig, A. H. Safavi-Naeini, O. Painter, and F. Marquardt, Phys. Rev. Lett. **109**, 063601 (2012).
[13] X.-Y. Lü, W.-M. Zhang, S. Ashhab, Y. Wu, and F. Nori, Sci. Rep. **3**, 2943 (2013).
[14] J. Ma, C. You, L.-G. Si, H. Xiong, J. Li, X. Yang, and Y. Wu, Phys. Rev. A **90**, 043839 (2014).
[15] G. S. Agarwal and S. Huang, Phys. Rev. A **81**, 041803(R) (2010).

[16] S. Weis, R. Riviere, S. Deleglise, E. Gavartin, O. Arcizet, A. Schliesser, and T. J. Kippenberg, Science **330**, 1520 (2010).
[17] A. H. Safavi-Naeini, T. P. Mayer Alegre, J. Chan, M. Eichenfield, M. Winger, Q. Lin, J. T. Hill, D. Chang, and O. Painter, Nature (London) **472**, 69 (2011).
[18] K. Qu and G. S. Agarwal, Phys. Rev. A **87**, 031802(R) (2013).
[19] Zhang-qi Yin and Y.-J. Han, Phys. Rev. A **79**, 024301 (2009).
[20] P. Kómár, S. D. Bennett, K. Stannigel, S. J. M. Habraken, P. Rabl, P. Zoller, and M. D. Lukin, Phys. Rev. A **87**, 013839 (2013).
[21] H. Miao, S. Danilishin, T. Corbitt, and Y. Chen, Phys. Rev. Lett. **103**, 100402 (2009).
[22] C. Jiang, H. Liu, Y. Cui, X. Li, G. Chen, and X. Shuai, Phys. Rev. A **88**, 055801 (2013).
[23] S. Huang and G. S. Agarwal, New J. Phys. **11**, 103044 (2009).
[24] A. H. Safavi-Naeini and O. Painter, New J. Phys. **13**, 013017 (2011).
[25] K. Stannigel, P. Komar, S. J. M. Habraken, S. D. Bennett, M. D. Lukin, P. Zoller, and P. Rabl, Phys. Rev. Lett. **109**, 013603 (2012).
[26] S. E. Harris, Phys. Today **50**(7), 36 (1997); K.-J. Boller, A. Imamoğlu, and S. E. Harris, Phys. Rev. Lett. **66**, 2593 (1991).
[27] H. Xiong, L.-G. Si, A.-S. Zheng, X. Yang, and Y. Wu, Phys. Rev. A **86**, 013815 (2012).
[28] M.-A. Lemonde, N. Didier, and A. A. Clerk, Phys. Rev. Lett. **111**, 053602 (2013).
[29] K. Børkje, A. Nunnenkamp, J. D. Teufel, and S. M. Girvin, Phys. Rev. Lett. **111**, 053603 (2013).
[30] A. Kronwald and F. Marquardt, Phys. Rev. Lett. **111**, 133601 (2013).
[31] S. Huang and G. S. Agarwal, Phys. Rev. A **83**, 023823 (2011).
[32] M. Karuza, C. Biancofiore, M. Bawaj, C. Molinelli, M. Galassi, R. Natali, P. Tombesi, G. Di Giuseppe, and D. Vitali, Phys. Rev. A **88**, 013804 (2013).
[33] H. Wang, X. Gu, Yu-xi Liu, A. Miranowicz, and F. Nori, Phys. Rev. A **90**, 023817 (2014).
[34] K. Qu and G. S. Agarwal, arXiv:1210.4067.
[35] J. T. Hill, A. H. Safavi-Naeini, J. Chan, and O. Painter, Nat. Commun. **3**, 1196 (2012).
[36] C. Jiang, H. Liu, Y. Cui, X. Li, G. Chen, and B. Chen, Opt. Express **21**, 12165 (2013).
[37] Y. Guo, K. Li, W. Nie, and Y. Li, Phys. Rev. A **90**, 053841 (2014).
[38] P.-C. Ma, J.-Q. Zhang, Y. Xiao, M. Feng, and Z.-M. Zhang, Phys. Rev. A **90**, 043825 (2014).
[39] S. Shahidani, M. H. Naderi, and M. Soltanolkotabi, Phys. Rev. A **88**, 053813 (2013).
[40] J. M. Dobrindt, I. Wilson-Rae, and T. J. Kippenberg, Phys. Rev. Lett. **101**, 263602 (2008).
[41] S. Gröblacher, K. Hammerer, M. R. Vanner, and M. Aspelmeyer, Nature (London) **460**, 724 (2009).
[42] J. Ma, C. You, L.-G. Si, H. Xiong, X. Yang, and Y. Wu, Opt. Lett. **39**, 6931 (2014).
[43] D. K. Armani, T. J. Kippenberg, S. M. Spillane, and K. J. Vahala, Nature (London) **421**, 925 (2003).
[44] Y. Tanaka, T. Asano, and S. Noda, J. Lightwave Technol. **26**, 1532 (2008).
[45] M. Eichenfield, J. Chan, R. M. Camacho, K. J. Vahala, and O. Painter, Nature (London) **462**, 78 (2009).